NSF GRANT #0556161 Gas Phase Nanowire Integration Process
NSF PROGRAM NAME: NANOMANUFACTURING

ZnO Nanorod LEDs and Silicon Nanowire Integration

Lead P.I. Heiko O. Jacobs
University of Minnesota - Electrical Engineering

Chris Smith, Jesse Cole, Xinyu Wang
University of Minnesota - Electrical Engineering

Abstract: This article reports on the growth and integration of ZnO and Si nanowires sponsored under this grant. The first part was carried out by Xinyu Wang and is completed. It reports ZnO growth for the formation of nanorod LED arrays on Mg-doped p-GaN films. The electroluminescence spectra under forward and reverse bias were found to be distinctly different. Forward bias showed two peaks centered around 390 nm and 585 nm, while reverse bias showed a single peak at 510 nm. Forward bias transport and luminescence were attributed to hole injection from the GaN into the ZnO and recombination at defect states inside the ZnO yielding distinct color variations between individual wires. The color variations, defect emission, and quality of the ZnO has been improved in a separate study [see progress report for #0621137 and [1, 2]]. The second part carried out by Chris Smith reports on post processing of VLS grown silicon nanowires to gain control over location, density, diameter and orientation. Preliminary results on the proposed nanorotation and nanotransfer are presented which require further improvement.

1. Introduction: Nanowire components remain attractive building blocks for photovoltaic devices [3], biocompatible electrodes [4], DNA detectors [5], nanowire based resonant tunneling diodes [6], and field effect transistors [7], to name a few. First device prototypes have been realized in many research groups focusing on the size dependency of singe nanocomponents. The transition of device prototypes to products would require a nanomanufacturing platform which enables large area integration using parallel techniques to localize the nanocomponents at predetermined locations on low temperature flexible substrates. Control over location, size, and orientation are desired aspects of such a nanomanufacturing platform and progress has been made recently where control of some aspects have been achieved for materials such as InAs [8], ZnO [9], GaAs [10] and Si [11]. The research under this grant aims to increase the level of control and is presently limited to ZnO and Si nanorods and nanowires.

2. ZnO Nanorod LEDs: The first part of this letter explores ZnO nanorods and their use as LEDs on p-type GaN. There have been conflicting reports on the nature of the emission mechanism where some have reported electroluminescence (EL) [12] under reverse bias while others have reported forward bias emission [13]. Previous reports have shown a wide range of emission peaks which were attributed to variations in the dimensions or level of defects between nanorods. The variations illustrate an integration challenge which could benefit from an increased level of control. This paper reports EL emissions under both forward and reverse bias. Analysis of the photoluminescence and electroluminescence spectra suggests different injection mechanisms and locations of electron-hole recombination, which may help understand the nature of the previously conflicting results. Forward bias emission spectroscopy shows two peaks centered around 390 nm and 585 nm, while reverse bias emission shows a single peak at 510 nm. Reverse bias transport and luminescence were attributed to hot-hole injection from the ZnO nanorods into the GaN film through tunneling breakdown. Forward bias transport and luminescence are attributed to hole injection from the GaN into the ZnO and recombination at defect states inside the ZnO yielding distinct color variations between individual wires. The observation of ring shaped EL pattern and distinct colors of individual nanorods are discussed to point out the limitations of the currently known growth methods. The limitations of previously known growth methods has been dramatically improved through the discovery of a new nucleation process which allowed us to dramatically increase the uniformity, color variations, defect emission, and quality of the ZnO which is reported in a separate study [see progress report for #0621137 and [1, 2]].

The p-GaN templates were prepared by growing a 1 μm thick, highly Mg-doped GaN film on 0.7 μm of resistive GaN grown on a 30 nm thick AlN buffer layer on a c-plane sapphire substrate using RF plasma-assisted molecular beam epitaxy (MBE). The Hall measurements indicated that the hole concentration and

mobility of the p-GaN film were 6 x 10^{17} cm^{-3} and 9 $cm^2/V \cdot s$, respectively. The resistivity of the film was also measured as 1.2 ohm-cm. The ZnO nanorods were grown on Mg-doped GaN films using a solution method [14]. In brief, ZnO seeds were firstly formed on p-GaN substrate by spinning 1mM zinc acetate in ethanol followed by heat treatment in air at 350 ºC for 20 min. The vertically aligned ZnO nanorods were then grown on the seeded p-GaN film in 25 mM aqueous solution of zinc acetate and hexamine at 95 ºC for 1 h.

Figure 1 shows a schematic of the device along with a representative TEM and SEM images. The ZnO nanorods are of high crystallinity, as evidenced by XRD and HR-TEM (Fig. 1(a)). The average diameter and length of ZnO nanorods are approximately 80 nm and 1 µm, respectively (Fig. 1c). Figure 1b shows the device structure. To form the illustrated insulating matrix surrounding the ZnO nanorods, we deposited a 1.5 µm thin layer of SiO_2 onto the structure by plasma enhanced chemical vapor deposition (PECVD) at 340 ºC at a deposition rate as 40 nm/min, followed by tripod polishing and plasma etching to expose ZnO tips. A portion of the GaN film was masked using photoresist during this process to reserve a window to form a contact to the GaN film. The contact to the GaN was formed using DC sputtered Ni (30nm) followed by Au (100 nm) and rapid thermal annealing in H_2(10%)/N_2(90%) at 500 ºC for 30 seconds. For contacts to ZnO nanorods, we RF-sputtered a transparent layer of indium tin oxide (ITO) through a shadow mask, defining a pad diameter of 500 µm. Fig.1(c) represents the SEM image taken at a location of a scratch to reveal the sandwich structure of ZnO between GaN and SiO_2 films prior to polishing.

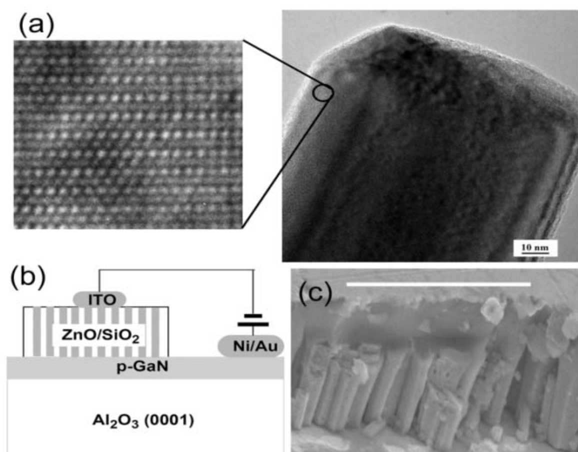

Figure 1. (a) High crystallinity evidenced by high resolution TEM, (b) heterojunction device structure, and (c) SEM image of ZnO nanorod array surrounded by SiO_2 on p-GaN, scale bar: 5 µm

Figure 2a compares the photoluminescence (PL) spectra of the isolated materials with the electroluminescence spectra of the fabricated device at room temperature. The PL spectrum of ZnO nanorods (silicon wafer as substrate) consists of an intense near-band-edge UV emission centered at 383 nm and a broad defect-related yellow band with much lower intensity near λ_{max} ~ 575 nm. The ZnO near-band-edge emission is attributed to the radiative annihilation of free and bound excitons [15]. In contrast, the PL spectrum of isolated GaN:Mg film consists of an intense near-band-edge band with λ_{max} at 370 nm and a broad band with λ_{max} at 505 nm, which is generally observed in Mg-doped GaN films and is attributed to a radiative recombination involving Mg acceptors [16]. The EL spectra was recorded using a scanning monochromator and photomultiplier tube attached to an upright microscope to record EL spectra from selected areas with a minimal spot size of 100 µm. Under forward bias, the EL spectrum showed two emission peaks: a UV emission centered at 390 nm and a broad, yellow-reddish emission with a maximum (λ_{max}) at 585 nm. The reverse bias EL exhibited a broad peak centered at 510 nm with a small shoulder in the UV at 380 nm.

The comparison between the EL and PL spectra yields the following observation: The forward bias EL spectrum matches the PL spectrum of the ZnO wires, whereas the reverse bias EL spectrum exhibited peak and shoulder locations that match the PL of the GaN. The location of these peaks suggest that under reverse bias electrons and holes recombined predominantly in the p-GaN film, indicating that the EL mechanism differs from conventional forward-biased LEDs.

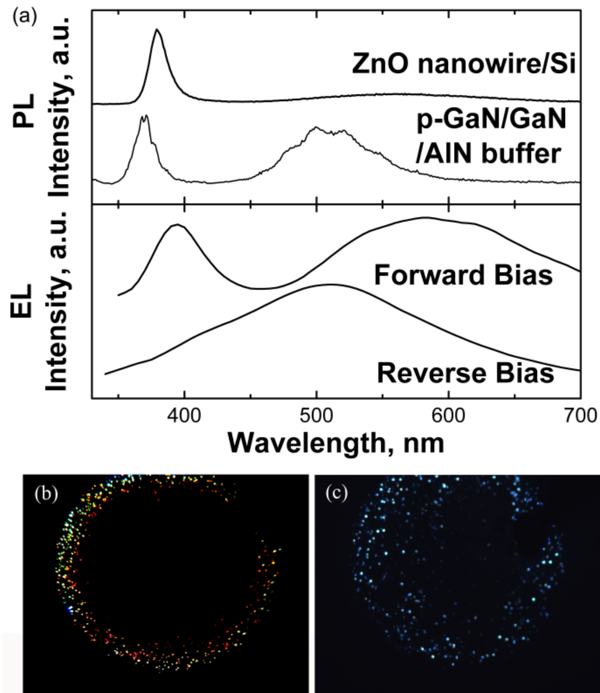

Figure 2. (a) PL spectra of ZnO nanorod arrays and p-GaN film and EL spectra of ZnO nanorod/p-GaN film heterojunction, (b) and (c) top view image (100x) micrograph of EL emission under forward and reverse bias, respectively.

Figure 2 (b) and (c) show a top view side-by-side comparison of the actual array at 100 x magnification recorded using a CCD camera without changing the capture settings. The individual dots represent emission of a single or clusters containing ~2-5 wires. The emission is not uniform, forward bias emission occurred primarily in a belt towards the edge of the ITO pad showing a small red shift towards the center of the pad. This effect was less pronounced under reverse bias. The color of the EL under reverse bias was bluish green and more nanorods showed emission towards the inner part of the ITO pad with less variation in color. The formation of the illuminated belt under forward bias is explained as in-plane ohmic losses inside the GaN film resulting in a potential drop towards the center region below the required 3V forward bias threshold. The larger threshold voltage (5V) under reverse bias reduces this effect. The actual lifetime of the device has not been determined, however, no noticeable device degradation has been observed over six months operating the device on average once a week for 10 minutes.

The I-V characteristic of the fabricated ZnO nanorod/p-GaN heterostructure is shown in Fig. 3. A turn on voltage of ~ 3V, leakage current of 1μA, and reverse bias breakdown voltage of 5 V was recorded. The linear portion in the I-V characteristic reveals a large series resistance of 10.8 kΩ. This resistance is caused primarily by the sheet resistance of p-GaN which was determined to be $12x10^3$ Ω/cm^2 by Hall measurement; the illustrated device used a 5 mm wide contact to the GaN film that was located ~ 0.7 mm away from the active area. The influences of the nanorod length and the ITO top contact on the I-V characteristic were insignificant. We doubled the length of the nanorods and did not see a measurable reduction in the current; ITO/ZnO nanorod/ITO test structures showed close to linear I-V characteristics with 50 times smaller differential resistance (~200 Ω per 0.05 cm^2 sized area) suggesting that the ITO/ZnO junction is not dominating the recorded transport. A similar measurement was carried out for the Au-Ni /GaN film/Ni-Au with the same contact layouts. The differential resistance (~10 kΩ) is comparable to that of the actual device. Considering these results we suggest that the non-linear diode like portions in the I-V curve of the actual device are caused by the ZnO/GaN heterojunction alone. The insert of Fig. 3 represents the re-plotted I-V curve by subtracting the series resistance of the GaN film. The recorded transport under forward and reverse bias can be explained in terms of band alignment of n-ZnO/p-GaN heterojunction at the interface.

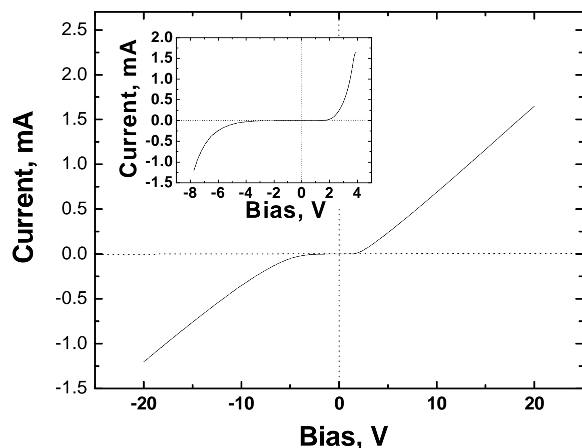

Figure 3. I-V characteristic of ZnO nanorod/p-GaN film heterojunction. Insert: Series resistance corrected I-V.

Under forward bias, holes are expected to be injected from p-GaN into the ZnO nanorods since the energy barrier for holes is less than the barrier for electrons at the heterojunction interface. While this appears to be the case considering the EL spectra we note that the estimated difference in energy barriers (0.13 eV for holes vs. 0.15 eV for electrons) is not significant enough

to guarantee injection and recombination exclusively in the ZnO nanorods. Other elements, such as defect states at the ZnO surface and heterojunction interface will play an important role and require further investigation. Another interesting element under forward bias is the variation in the color between individual wires. We cannot explain this variation by quantum size effects or by statistical variation of the number of states and recombination centers and types inside the wire. Instead we believe that the observed variation is due to different current densities caused by variations in the contact resistance from wire to wire. Wires carrying a high current density due to a reduced contact resistance would involve filling of all states including defect states and near-band-edge states. This explanation is consistent with average emission shifting towards longer wavelength towards the center of the contact where the voltage has dropped due to the in-plane sheet resistance of the GaN film.

As for the EL emission from reverse bias, the mechanism of hole injection and recombination is still under debate. The breakdown mechanism follows the equation derived [17] for tunneling breakdown,

$$J_z = aV^2 \exp\left(-\frac{b}{V}\right)$$

where a and b are constants related to the energy bandgap and doping concentration. The calculated I-V curve shows good agreement for small and medium bias (Figure 4), which is an indication of tunneling breakdown due to the thinning of energy barrier of interface under reverse bias. The actual current begins to exceed the values predicted by tunneling breakdown at high bias suggesting and additional avalanche breakdown component. Pre-breakdown electroluminescence has been reported previously in reversed biased GaN based thin film devices [18].Accordingly, following a similar argumentation but considering the ZnO nanorod / GaN thin film heterojunction, hot holes are injected from the ZnO conduction band into the GaN valence band and excite electrons from the GaN valence band into the GaN conduction band. Excitation could be enhanced by GaN defects and by confinement of electrons via bandgap differences in the heterojunction.

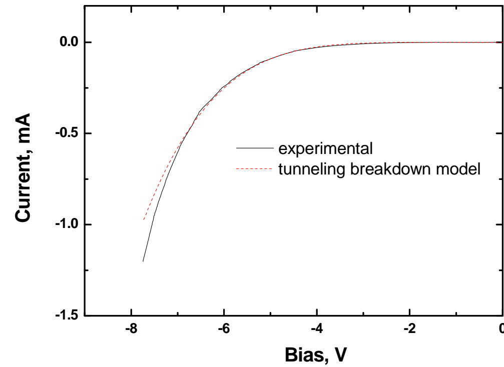

Figure 4. Comparison of the experimental and calculated reverse bias I-V curve considering tunneling breakdown.

The results illustrate that the ZnO nanorods have a poor quality considering the optical emission. These color variations, defect emission, and quality of the ZnO has been dramatically improved in a separate study [see progress report for #0621137 and [1, 2]. The commonly observed defect related emission in the electroluminescence spectra is completely suppressed, and a single near-band-edge UV peak is observed in most recent results (Fig 5) [1, 2].

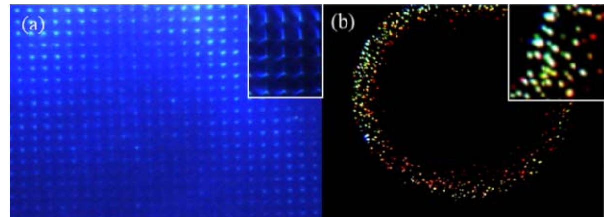

Figure 5. (A) ZnO crystals grown on oxygen plasma treated GaN exhibited lower pinhole defects and single peak UV electroluminescence when compared to (B) ZnO nanowires grown on untreated samples had originally emitted in the yellow.

3. Silicon nanowire integration: The second part of this study explores silicon nanowires and their use for printable electronics. The possible extension from Si based microelectronics to macroelectronics where minimal amounts of Si has to be distributed over large areas poses a challenge to the field of nanomanufacturing. Specifically, it has been difficult to create complex crystalline interconnected networks of silicon nanowires on flexible substrates with control over the size, location, and orientation on an individual nanocomponent basis. The field would benefit from an increased level of control and an extension to larger areas.

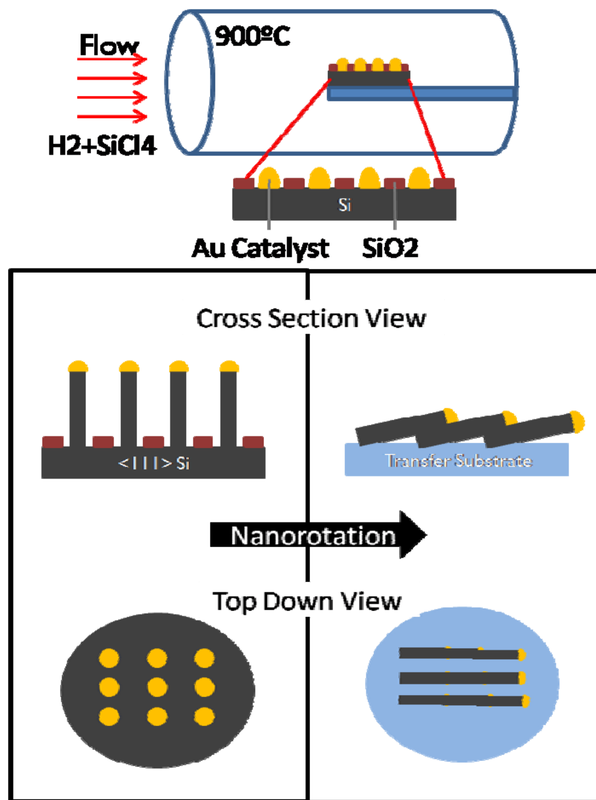

Figure 6. Si nanowires were synthesized by the VLS technique using the thermal decomposition of silicon tetrachloride in the presence of hydrogen. Nanowires are then oriented horizontally and transferred using the nanorotation method.

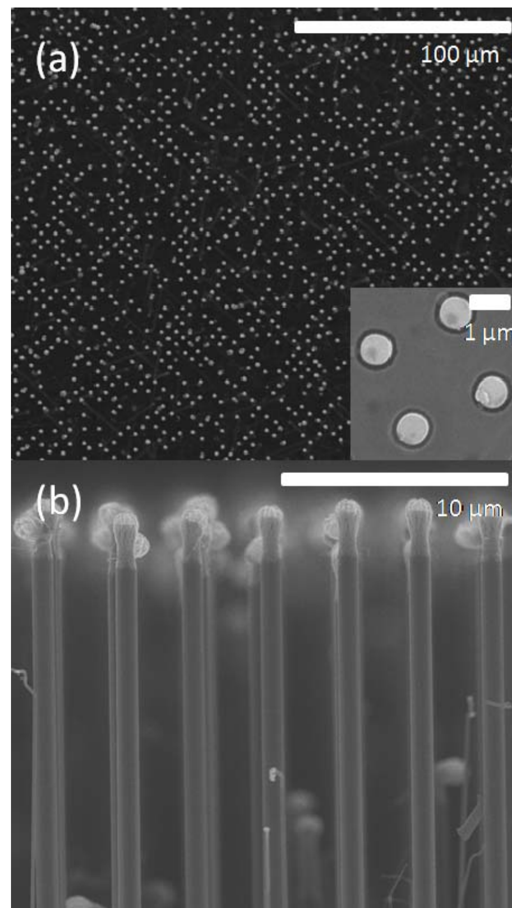

Figure 7. (a) Top down image of silicon nanowires at specific growth sites from Au catalysts (inset). (b) Cross section of nanowires with uniform length and vertical orientation.

Figure 6 shows originally proposed post-processing of VLS grown Si nanowires. While this idea dates back to 2005 yielding preliminary results, the improvement of the yield beyond original results has been difficult. We utilize a growth process similar to previously reported methods where silicon tetrachloride ($SiCl_4$) is used as the precursor gas with H_2 as the carrier, but optimal growth occurs at temperatures below 1000 degrees C whereas previous studies report optimal growth above 1000 degrees C [11]. The prepared substrate is gently rinsed with isopropyl alcohol and placed into a horizontal tube furnace then the furnace chamber is purged with H_2 at a flow rate of 1900SCCM for 20 minutes. Next, the furnace temperature is ramped from room temperature to temperatures ranging from 800-1000 degrees Celsius, followed by a 10-30 minute annealing step to ensure alloying between the Au catalyst and the silicon substrate. This is followed by a 10-30 minute growth step in which H_2 is flown through liquid $SiCl_4$ in a bubbler to deliver the silicon precursor gas to the growth substrate. Once the growth process is complete, the furnace is quickly cooled while maintaining the flow of H_2. The growth substrate is then removed from the furnace. The focus of this work has been on the post processing steps to tailor the lengths (not shown), orientation (shown), and final substrate material (not shown). Preliminary results on nanorotation are included in this progress report. Nanorotation involves the use of a micromanipulator to bring the two surfaces in contact while providing a translational motion. Specifically, we use PDMS which is brought in contact with the tops of the nanowires to apply a shear force to rotate the nanowires into a predefined horizontal direction. The forces between the nanowires and the transfer substrate cause the nanowires to tilt and ultimately break free from the growth substrate. The details of this process are presently under investigation and will be published separately once sufficiently understood.

Figure 7 shows the results of the VLS grown nanowires in the vertical orientation. Location and density are controlled through proper placement of catalyst material, while length is controlled by varying the growth time. On average, each catalyst site produces a single nanowire with uniform diameter and orientation although not all Au catalysts will create wires along the <111> crystal direction. Some of the Au catalyst sites

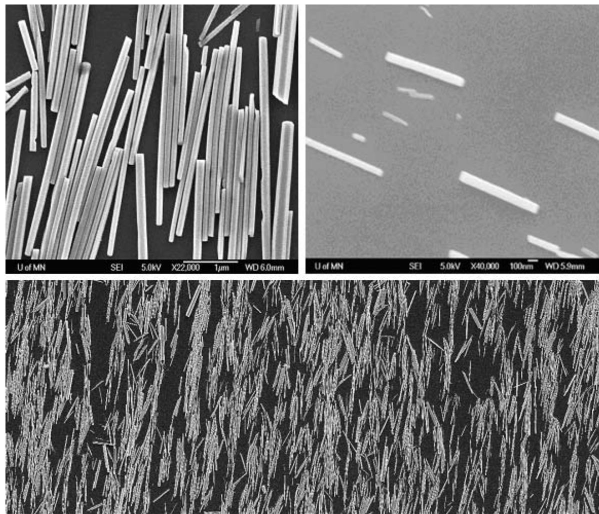

Fig 8. Initial result showing a top view SEM of ZnO nanowire after nanorotation

produce nanowires with random orientation and diameter which may be controlled through further process optimization. The wires also have Au tips with a flower-like structure, which is a characteristic of the VLS process due to the oxidation of the Au particle at the interface.

Figure 8 shows first results of some oriented nanowires produced using nanorotation. The results require further improvement. The next steps are geared at optimizing the growth parameters and nanorotation procedures to increase the yield of the process.

4. Conclusion: ZnO nanowire array/p-GaN film heterojunction diodes were fabricated and their optical properties were evaluated. EL emission emerged under both forward and reverse bias. Contrary to conventional injection under forward bias, tunneling break-down occurred under reverse bias and electron-hole recombination was found to take place in the p-GaN film. The observation of ring shaped EL pattern and distinct colors of individual nanowires pointed out an interesting integration challenge which has been addressed in a separate study [see progress report for #0621137 and [1, 2]] producing ZnO LEDs of higher quality and uniform emission where defect peek emission has been eliminated. Present research under this grant investigates the integration and post processing of Si nanowires.

5. Acknowledgments: We acknowledge support of this work by NSF DMI-0556161.

6. References:

[1] J. Cole, X. Wang, R. Knuesel, and H. Jacobs, *Adv. Mater*, vol. 20, pp. 1474-1478, 2008.

[2] J. Cole, X. Wang, R. Knuesel, and H. Jacobs, *Nano Lett*, vol. 8, pp. 1477-1481, 2008.

[3] T. Kempa, B. Tian, D. Kim, J. Hu, X. Zheng, and C. Lieber, *Nano Letters*, vol. 8, pp. 3456-3460, 2008.

[4] J. Martinez, N. Misra, Y. Wang, P. Stroeve, C. Grigoropoulos, and A. Noy, *Nano Letters*, vol. 9, pp. 914-918, 2009.

[5] Z. Gao, A. Agarwal, A. Trigg, N. Singh, C. Fang, C. Tung, and K. Buddharaju, presented at Solid-State Sensors, Actuators and Microsystems Conference, 2007. TRANSDUCERS 2007. International, 2007.

[6] M. Björk, B. Ohlsson, T. Sass, A. Persson, C. Thelander, M. Magnusson, K. Deppert, L. Wallenberg, and L. Samuelson, *Applied Physics Letters*, vol. 80, pp. 1058, 2002.

[7] D. Khanal and J. Wu, *Nano Lett*, vol. 7, pp. 2778-2783, 2007.

[8] K. Dick, K. Deppert, L. Karlsson, W. Seifert, L. Wallenberg, and L. Samuelson, *Nano Lett*, vol. 6, pp. 2842-2847, 2006.

[9] J. Zuniga-Perez, A. Rahm, C. Czekalla, J. Lenzner, M. Lorenz, and M. Grundmann, *Nanotechnology*, vol. 18, pp. 195303-195303, 2007.

[10] Z. Wu, M. Hahm, Y. Jung, and L. Menon, *Journal of Materials Chemistry*, vol. 19, pp. 463-467, 2009.

[11] B. Kayes, M. Filler, M. Putnam, M. Kelzenberg, N. Lewis, and H. Atwater, *Applied Physics Letters*, vol. 91, pp. 103110, 2007.

[12] W. Park and G. Yi, *Advanced Materials*, vol. 16, pp. 87-90, 2004.

[13] M. Jeong, B. Oh, M. Ham, and J. Myoung, *Applied Physics Letters*, vol. 88, 2006.

[14] L. Greene, M. Law, D. Tan, M. Montano, J. Goldberger, G. Somorjai, and P. Yang, *Nano Lett*, vol. 5, pp. 1231-1236, 2005.

[15] P. Zu, Z. Tang, G. Wong, M. Kawasaki, A. Ohtomo, H. Koinuma, and Y. Segawa, *Solid State Communications*, vol. 103, pp. 459-464, 1997.

[16] M. Khan, Q. Chen, R. Skogman, and J. Kuznia, *Applied Physics Letters*, vol. 66, pp. 2046, 1995.

[17] R. Bhan and V. Gopal, *Semiconductor Science and Technology*, vol. 9, pp. 289-289, 1994.

[18] D. Starikov, I. Berichev, N. Medelci, E. Kim, Y. Wang, and A. Bensaoula, presented at AIP Conference Proceedings, 1998.

[19] S. Acharya, A. Panda, N. Belman, S. Efrima, and Y. Golan, *Advanced Materials*, vol. 18, pp. 210-212, 2006.